An Experimental Investigation of Wideband MIMO Channel Based on Indoor Hotspot NLOS Measurements at 2.35GHz

Xin Nie[1], Jianhua Zhang[1], Yu Zhang [1], Guangyi Liu[2], Zemin Liu [1]
[1]Key Lab. of Universal Wireless Communications, Ministry of Education
Beijing Univ. of Posts and Telecommunications, P.O. box #92, China, 100876
Email: niexin@mail.wtilabs.cn, jhzhang@bupt.edu.cn
[2] Research Institute of China Mobile, Beijing, China, 100053

***Abstract*—In this paper, measurement data from wideband Multiple-Input Multiple-Output (MIMO) channel measurements at 2.35GHz are presented. Measurements were preformed in indoor hotspot scenario with no line of sight (NLOS). Space-Alternating Generalized Expectation (SAGE) algorithm was utilized to estimate angular domain parameters and powers of multipath components (MPCs), which are then used to compute the circular angular spread (CAS) and to construct the power azimuth spectrum (PAS) of transmitter and receiver sides. It is found that PASs of both sides follow multi-cluster truncated Laplacian distribution. The spatial correlation, capacity and multiplexing gain are also presented. Due to rich scatters in the indoor hotspot environment, the correlation space is 0.2λ and the multiplexing gain is 15, which indicate indoor hotspot MIMO channels facilitate multiplexing and could achieve high capacity. The results provide important basis for future channel modeling and technique evaluation.**

I. Introduction

Accurate parameter analysis and channel modeling is vital for the study and deployment of future transmission technology. MIMO, which promises high spectral efficiency and reliability [1], is one of the most promising 4G candidate technologies. Performance of MIMO system, i.e. capacity and spatial multiplexing, are all essentially influenced by statistics of propagation channel between transmitter (Tx) array and receiver (Rx) array.

High data rate services are common in a hotspot area with heavy traffic and high user density, i.e. conference halls, shopping malls and airports. Therefore, an important application of MIMO system occurs in indoor hotspot scenario where both transmitter and receiver are surrounded by local scatters.

Radio propagation measurements in the indoor radio channel were reported by several researchers [2-4]. These measurements were conducted in different indoor scenarios at frequencies 2GHz, 5.8GHz and 60 GHz and most of the researchers focused on the fading statistics and time domain parameters. In [5], the power delay profiles and path numbers at 2.55G and 5.25G were compared. A channel measurement for wireless sensor applications at 2.6GHz was reported in [6].

We conducted a measurement campaign to explore the statistics of indoor hotspot MIMO channel in frequency band between 2.3GHz and 2.4GHz in China. In our measurement, a time multiplexing mode (TDM) based channel sounder is employed. The Tx is a 3D cylindrical omni-directional array (ODA), which consists of 56 dual-polarized patch elements, while the Rx is a uniform planar array (UPA) with 32 dual-polarized patch elements. In order to reveal the particular characteristic of MIMO channel, we focus on the parameters of angular and spatial domain.

The remainder of this paper is organized as follows: Section II describes the measurement equipments and scenario. Section III presents the procedure of post data processing. Section IV presents the result of parameter analysis. CAS, PAS, spatial correlation, capacity and the multiplexing gain of channels are shown. Section V gives the conclusion of our work.

II. Measurement

An extensive measurement campaign was performed at center frequency of 2.35GHz with 100MHz bandwidth at *Beijing University of Posts and Telecommunications (BUPT), Beijing, China*.

A. Equipment

The Elektrobit PropSound Channel Sounder [7] was employed. The sounder is described in more detail in [8]. The sounder worked in a TDM mode. Periodic pseudo random binary signals were transmitted between different Tx-Rx antenna pairs. The interval within which all sub-channels are sounded once is referred to as a measurement cycle.

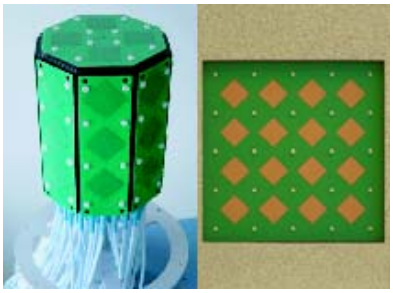

(a) (b)

Fig.1. Antenna arrays used in measurement (a)Tx ODA (b)Rx UPA

978-1-4244-2324-8/08/$25.00 © 2008 IEEE.

This full text paper was peer reviewed at the direction of IEEE Communications Society subject matter experts for publication in the IEEE "GLOBECOM" 2008 proceedings.

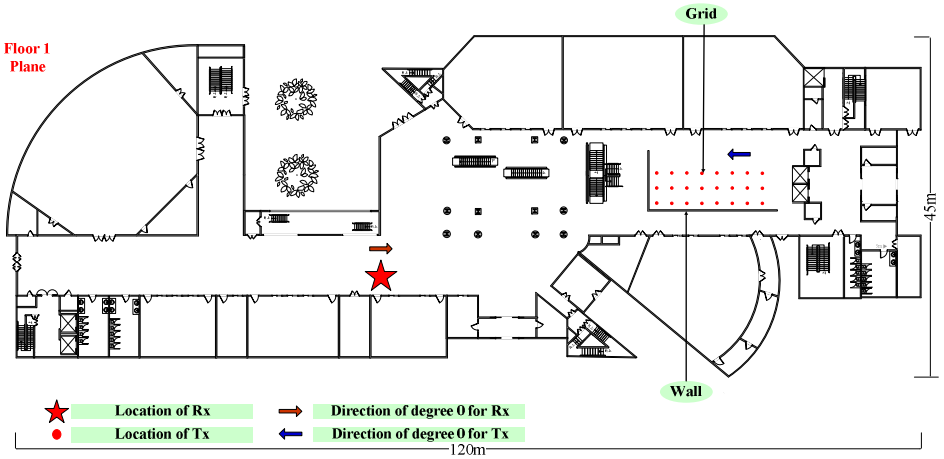

Fig.2. Indoor hotspot measurement scenario

The Tx array with 56 elements is shown in Fig. 1(a). Two rings of the elements were used, namely, 32 dual-polarized patch elements. Fig. 1(b) illustrates the Rx array with 32 elements, 16 of which were used. Due to the geometry of antenna arrays, both the Tx and the Rx support azimuth and elevation probing. Summary of parameters is given in Table I.

TABEL I
MEASUREMENT PARAMETERS

Items	Settings
Carrier frequency[GHz]	2.35
Bandwidth[MHz]	100
Chip Rate[MHz]	100
Code length[Chips]	511
Cycle Rate[Hz]	20
Tx power[dBm]	33
Number of Tx antenna	32
Number of Rx antenna	16
Height of Tx antenna[m]	1.05
Height of Rx antenna[m]	2.5

B. Scenario

A seven-floor building was selected as the measurement site. The measurements were carried out in the large hall on the first floor of the building. Floors and the sidewalls of the corridor were covered with marbles. There were also several notice boards with glass sheets along both sides of the corridor. Between the Tx and the Rx, there were huge concrete poles, escalators, a staircase with aluminum banisters, notice boards with glass sheets, etc, which blocked the direct path from the Tx to the Rx. No line of sight existed between the Tx and the Rx. People were moving around in the hall during the measurement.

Layout of the hall is illustrated in Fig.2. Both the Tx and the Rx were mounted on the trolley. The star mark indicates the position where the Rx was fixed. Meanwhile, the Tx was moved to every spot denoted by red dot in the grid. At each spot 100 measurement cycles were transmitted and collected. In total, 24×100=2400 measurement cycles were obtained.

III. POST DATA PROCESSING

Post data processing consists of two procedures: 1) obtaining channel impulse response (CIR) from raw data, 2) extracting channel parameters using Space-Alternating Generalized Expectation algorithm [9].

A. Channel Impulse Response

Raw data collected in the Rx is the spread signals with the system impulse response of the sounding system. Raw data were cyclically correlated with the system impulse response, which was obtained from the calibration of the sounder, to remove the effect of the sounding system. Then, CIRs were obtained through the cyclic correlation with the known PN codes. In order to satisfy the wide-sense stationary and uncorrelated scattering (WSSUS) condition, the CIRs for a sub-channel were divided into subsets, and averaged according to

$$h_{av}(\tau) = E_t\{h(t,\tau)\} \quad (1)$$

where $E_t\{\bullet\}$ denotes the average in time domain.

The squared CIRs of all sub-channels of the 32×16 MIMO system were averaged to generate one channel realization. The dynamic range for the averaged CIR was set to 30dB and the noise floor was dynamically removed.

B. Parameter Extraction with SAGE

SAGE, which is well suited for MIMO channel parameter extraction, is used to extract the channel parameters. SAGE is based on the maximum likelihood (ML) method and allows joint estimation of parameter set $\theta_l = [\Omega_{1,l}, \Omega_{2,l}, \tau_l, \nu_l, \alpha_l]$ of l^{th} propagation path from the CIR. $\Omega_{1,l}, \Omega_{2,l}, \tau_l, \nu_l, \alpha_l$ denote direction of departure, direction of incidence, propagation delay, dropper shift, and complex weight, respectively. Every four snapshots of measurement data were fed to SAGE and one set of channel parameters was generated. In total, 600 SAGE results were obtained. In order to extract all the important paths that can correctly characterize the scenario, the upper bound of multipath number was set to 50. The resolutions of delay and angle were 1 degree and 5 ns, respectively.

This full text paper was peer reviewed at the direction of IEEE Communications Society subject matter experts for publication in the IEEE "GLOBECOM" 2008 proceedings.

IV. Numerical Results

Based on the CIRs and parameter extraction results of SAGE, the circular angular spread , power azimuth spectrum, spatial correlation, capacity and multiplexing gain of the scenario were analyzed.

A. Power Delay Profile

According to (1), the power delay profile is constructed. PDP of all measurement cycles is shown in Fig 3. PDP provides the information of propagation delay and multipath delay.

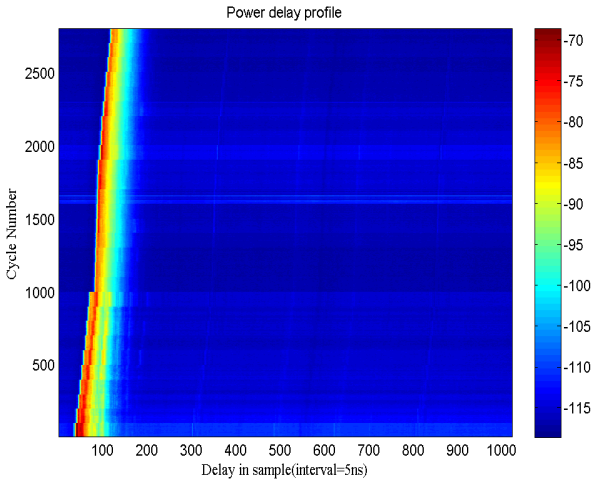

Fig.3. Power delay profile of measurement. Colors represent power in dB.

B. Circular Angular Spread

Angular spread is another important parameter for wireless system design. The angular information of propagation paths are estimated by SAGE. Circular angular spread σ_{AS} is defined as [10]

$$\sigma_{AS} = \min_{\Delta} \sigma_{AS}(\Delta) = \sqrt{\sum_{n=1}^{N} \left(\theta_{n,u}(\Delta)\right)^2 \bullet P_n \Big/ \sum_{n=1}^{N} P_n} \qquad (2)$$

where P_n is the energy of individual path. $\theta_{n,\mu}$ is defined as

$$\theta_{n,\mu}(\Delta) = \begin{cases} 2\pi + \left(\theta_n(\Delta) - \mu_\theta(\Delta)\right) & \left(\theta_n(\Delta) - \mu_\theta(\Delta)\right) < -\pi \\ \left(\theta_n(\Delta) - \mu_\theta(\Delta)\right) & \left|\left(\theta_n(\Delta) - \mu_\theta(\Delta)\right)\right| < \pi \\ 2\pi - \left(\theta_n(\Delta) - \mu_\theta(\Delta)\right) & \left(\theta_n(\Delta) - \mu_\theta(\Delta)\right) > \pi \end{cases} \qquad (3)$$

$\mu_\theta(\Delta)$ is defined as

$$\mu_\theta(\Delta) = \left(\sum_{n=1}^{N} \theta_n(\Delta) \bullet P_n\right) \Big/ \sum_{n=1}^{N} P_n \qquad (4)$$

$$\theta_n(\Delta) = \theta_n + \Delta \qquad (5)$$

where θ_n is the angle of n^{th} path and Δ denotes the angle ranging from $-\pi$ to π.

The cumulative distribution functions (CDF) of CASs are shown in Fig.4. The mean CAS of azimuth of departure (AOD), azimuth of arrival (AOA), elevation of departure (EOD) and elevation of arrival (EOA) are 57, 23, 17 and 6 degree. The barriers between Tx and Rx hamper paths heavily. So with high probability, MPCs transmit to the Rx via the reflection of side walls, ceiling and floor, resulting in a larger angular spread.

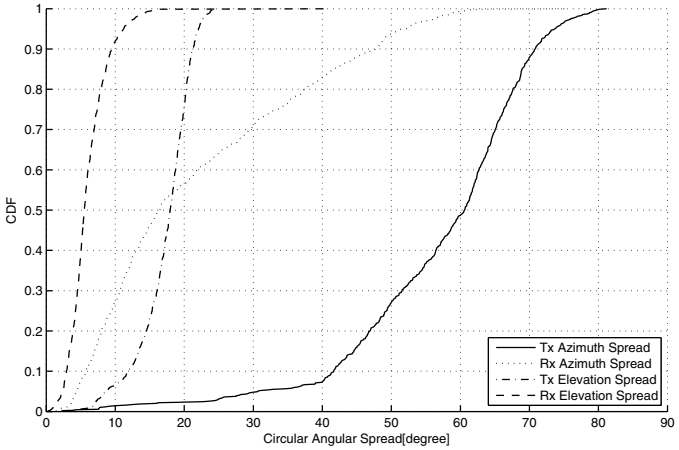

Fig.4. CDFs of AOD, AOA, EOD and EOA circular spread

C. Power Azimuth Spectrum

The Laplacian distribution has been introduced in [11] as the best fit to measurement results in urban and rural areas. In the case of MPCs gathering in several clusters, PAS can be described by a multi-cluster truncated distribution, which writes

$$PAS(\phi) = \sum_{k=1}^{Nc} \frac{Q_{L,k}}{\sigma_{L,k}\sqrt{2}} \exp\left[-\sqrt{2}\left|\phi - \phi_{0,k}\right| \Big/ \sigma_{L,k}\right] \bullet \left\{\varepsilon[\phi - (\phi_{0,k} - \Delta\phi_k)] - \varepsilon[\phi - (\phi_{0,k} + \Delta\phi_k)]\right\} \qquad (6)$$

where $\varepsilon(\phi)$ is the step function and N_c is the number of clusters. $\Delta\phi_k$ is the bound of angular in k^{th} cluster. $\phi_{0,k}$, $\sigma_{L,k}$ are the mean angle and angle spread of k^{th} cluster, respectively. The normalization const $Q_{L,k}$ is derived such that

$$\sum_{k=1}^{Nc} Q_{L,k}\left[1 - \exp\left(-\sqrt{2}\Delta\phi_k \Big/ \sigma_{L,k}\right)\right] = 1 \qquad (7)$$

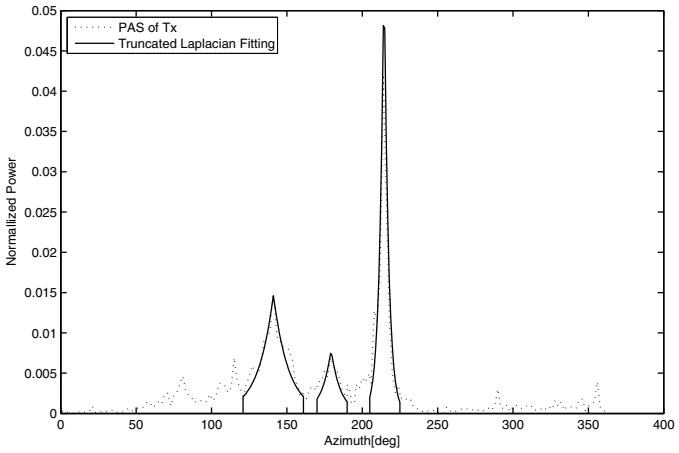

Fig.5. PAS of Tx Azimuth and multi-cluster truncated Laplacian fitting

TABLE II
Parameters of Tx PAS Clusters

k	$Q_{L,k}$	$\phi_{0,k}$ [deg]	$\Delta\phi_k$ [deg]	$\sigma_{L,k}$ [deg]
1	0.46	134.4	20	14.4
2	0.15	178.3	10	8.8
3	0.49	213.4	10	4.0

This full text paper was peer reviewed at the direction of IEEE Communications Society subject matter experts for publication in the IEEE "GLOBECOM" 2008 proceedings.

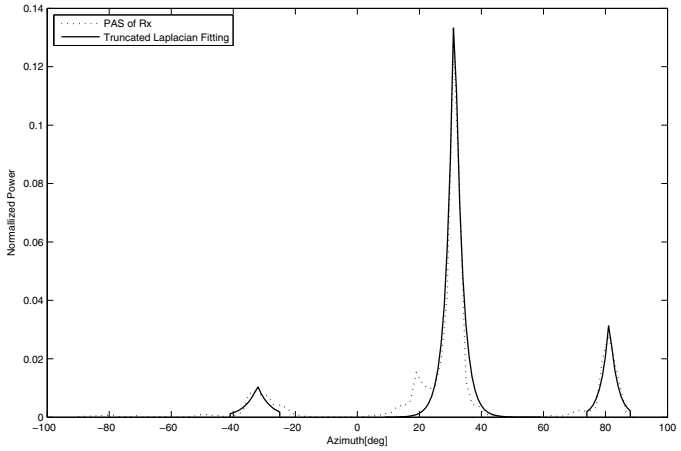

Fig.6. PAS of Rx Azimuth and multi-cluster truncated Laplacian fitting

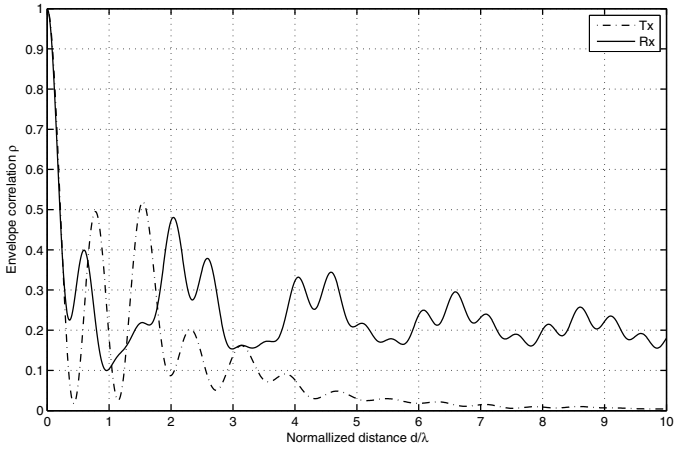

Fig.7. Spatial correlation of Tx and Rx versus normalized spacing

TABLE III
PARAMETERS OF RX PAS CLUSTERS

k	$Q_{L,k}$	$\phi_{0,k}$ [deg]	$\Delta\phi_k$ [deg]	$\sigma_{L,k}$ [deg]
1	0.09	-31.2	8	5.7
2	0.75	32.2	25	11.4
3	0.17	82.2	7	3.5

Fig.5 and Fig.6 show the PASs of the Tx and the Rx. The dashed line is the measured PAS obtained from SAGE results while the solid line is the corresponding multi-cluster truncated Laplacian fitting. Both the Tx and the Rx have three main power unbalanced clusters. Parameters for describing clusters of PAS are shown in TABEL II and III.

D. Spatial Correlation

The envelope correlation is commonly used to characterize the spatial selectivity of the channel. Assuming the multi-cluster truncated Laplacian PAS, The cross-correlation function writes [12]

$$R_{XX,L}(D)=J_0(D)+4\sum_{k=1}^{Nc}\frac{Q_{L,k}}{\sqrt{2}\sigma_{L,k}}\sum_{m=1}^{+\infty}\frac{J_{2m}(D)}{\left(\left(\frac{\sqrt{2}}{\sigma_{L,k}}\right)^2+(2m)^2\right)}\cos\left(2m\phi_{0,k}\right)$$
$$\bullet\left\{\frac{\sqrt{2}}{\sigma_{L,k}}+\exp\left(-\frac{\sqrt{2}\Delta\phi_k}{\sigma_{L,k}}\right)\left[2m\sin\left(2m\Delta\phi_k\right)-\frac{\sqrt{2}}{\sigma_{L,k}}\cos(2m\Delta\phi_k)\right]\right\} \quad (8)$$

$$R_{XY,L}(D)=4\sum_{k=1}^{Nc}\frac{Q_{L,k}}{\sqrt{2}\sigma_{L,k}}\sum_{m=1}^{+\infty}\frac{J_{2m+1}(D)}{\left(\left(\frac{\sqrt{2}}{\sigma_{L,k}}\right)^2+(2m+1)^2\right)}\sin\left[(2m+1)\phi_{0,k}\right]$$
$$\bullet\left\{\frac{\sqrt{2}}{\sigma_{L,k}}-\exp\left(-\frac{\sqrt{2}\Delta\phi_k}{\sigma_{L,k}}\right)\bullet\right.$$
$$\left.\left\{(2m+1)\sin\left((2m+1)\Delta\phi_k\right)+\frac{\sqrt{2}}{\sigma_{L,k}}\left[\cos(2m+1)\Delta\phi\right]\right\}\right\} \quad (9)$$

where $J_m(\bullet)$ is the Bessel function of the first kind and m^{th} order. The correlation coefficient of envelope is defined as

$$\rho_e(D)\triangleq\left|R_{XX}(D)+jR_{XY}(D)\right|^2 \quad (10)$$

The spatial correlation coefficients of envelop at the Tx and the Rx are shown in Fig.7. The spatial correlation at the Tx decreases rapidly as the antenna separation increases due to wide angle spread of the Tx PAS while the spatial correlation at the Rx is higher than Tx even for large antenna separation due to narrow angle spread of the Rx PAS.

The required antenna separation for $\rho_e(D)\le 0.7$ is known as the correlation space [13]. We can see from Fig.7 that the correlation space for the Tx and the Rx is 0.2λ. The spatial correlation is useful for array design to maximize the capacity.

E. Channel Capacity and Multiplexing Gain

Channel capacity is the main benefit resulted by applying MIMO for spatial multiplexing. The capacity of $N_T\times N_R$ frequency-selective fading MIMO channel is given by [14]

$$C=\frac{1}{B}\int_B\log_2\det\left(\mathbf{I}_{N_R}+\frac{\rho}{N_T}\mathbf{H}(f)\mathbf{H}(f)^H\right)df \quad (11)$$

where ρ denotes the signal-to-noise ratio (SNR), B is the bandwidth and $\mathbf{H}(f)$ is the frequency domain channel matrix. For each channel realization $\mathbf{H}_q$, an approximation can be given by

$$\tilde{C}(\rho)=\frac{1}{Q}\sum_{q=1}^{Q}\log_2\det\left(\mathbf{I}_{N_R}+\frac{\rho}{\beta N_T}\mathbf{H}_q\mathbf{H}_q^H\right) \quad (12)$$

where Q is the number of channel realizations and β is a common normalization factor for all channel realizations $\mathbf{H}_q$ in such that the average channel power gain is unitary [15], i.e.

$$E\left\{\frac{1}{\beta}\left\|\mathbf{H}_q\right\|_F^2\right\}=N_R\bullet N_T \quad (13)$$

$E\{\bullet\}$ is expectation operator over all channel realizations.

The CIRs between different Tx-Rx antenna pairs are used to form the channel transfer matrix. After transforming the transfer matrix to the frequency domain, we can calculate the capacity using (11). Fig.8 shows the capacity of 32×16 MIMO channels. The SNR ascends from left hand side to right hand side.

The multiplexing gain of MIMO channels is a measure of

This full text paper was peer reviewed at the direction of IEEE Communications Society subject matter experts for publication in the IEEE "GLOBECOM" 2008 proceedings.

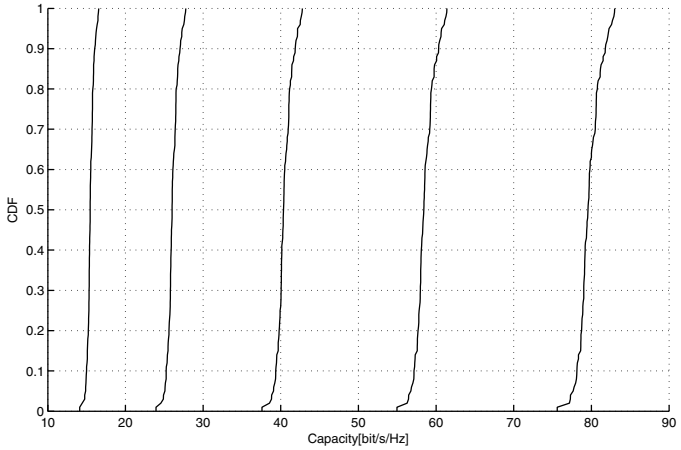

Fig.8. CDFs of Channel capacity at different SNR (from left to right, SNR=5, 10, 15, 20, 25dB, respectively)

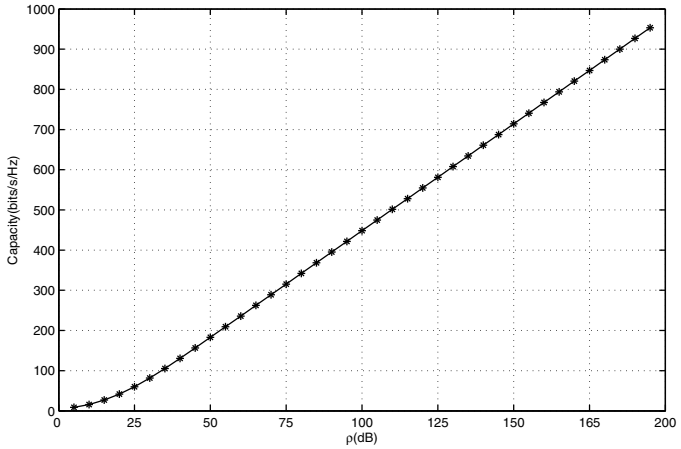

Fig.9. Channel capacity as a function of SNR, as ρ approaches ∞ , the slope of the curve indicates the multiplexing gain of channels.

capability for supporting higher data rate than single antenna channels. The multiplexing gain γ is defined as [16]

$$r = \lim_{\rho \to \infty} \frac{C}{\log_2 \rho} \tag{14}$$

where ρ is the SNR and C denotes ergodic capacity.

From Fig.9, we can obtain that the multiplexing gain of measured data is approximately 15, which approximately equals to minimum number of Tx and Rx antennas. The measured MIMO channel can be viewed as fifteen independent parallel channels. The result suggests that due to rich scatters in the indoor hotspot environment, MIMO channels facilitate multiplexing and can achieve high capacity.

V. Summary And Conclusions

This paper presents the result from wideband channel measurement at 2.35GHz of an indoor hotspot scenario. The circular angular spread of AOA, AOD, EOA and EOD are presented. Then the spatial correlation based on PAS of a multi-cluster truncated Laplacian distribution is analyzed. The correlation space for the Tx and the Rx is 0.2λ . NLOS and rich scatters result in a relatively larger angular spread and smaller correlation space. The channel capacity and multiplexing gain are also studied. The result shows that MIMO channels in indoor hotspot scenario facilitate multiplexing and could achieve high capacity. Due to the differences in frequency band, layout of buildings, building materials, user density, the propagation channel manifest different characteristics from former results. These results provide important basis for future studies of indoor hotspot propagation characteristics and MIMO system designs.

Acknowledgment

This work was funded in part by the National 863 High Technology Research and Development Program of China under Grant No.2006AA01Z258, and by Research Institute of China Mobile.

References

[1] E. Teletar, “Capacity of multi-antenna Gaussian channels,” *Europ Trans. Telecomm*, vol.6, pp 311-355, Mar.1998.

[2] G. J. M. Janssen, P. A. Stigter and R. Prasad, “Wideband indoor channel measurements and BER analysis of frequency selective multipath channels at 2.4, 4.75, and 11.5 GHz,” IEEE Trans. Commun., vol. 44, pp.1272-1288, Oct. 1996.

[3] H. Yang, P. F. M. Smulders and M.H.A. J. Herben, “Indoor channel measurements and analysis in the frequency bands 2 GHz and 60 GHz,” in *Proc. VTC’2005*, vol.1, pp.579-583, Sept. 2005.

[4] A. A. Ali, O. Aly and A.S. Omar, “High resolution WLAN indoor channel parameter estimation and measurements for communication and positioning applications at 2.4, 5.2 and 5.8 GHz,” in *Proc. IEEE Radio and wireless symposium 2006*, pp.279-282, Jan. 2006.

[5] W. Shurjeel, T. Santos, F. Tufvesson, A.F. Molisch, and F. Andreas, “Channel Measurements of an Indoor Office Scenario for Wireless Sensor Applications,” in *Proc. IEEE GlobalCom’2007*, pp.3831-3836, Nov. 2007.

[6] E. Bonek, N. Czink, V. Holappa, M. Alatossava, L. Hentilä, J. Nuutinen, and A. Pal, “Indoor MIMO measurements at 2.55 and 5.25 GHz – a comparison of temporal and angular characteristics,” in *Proc. IST Mobile Summit*, 2006.

[7] A. Stucki, Propsound system specifications document: Concept and specifications Elektrobit AG Tech. Rep., 2001.

[8] Propsound multidimensional channel sounder, Elektrobit Ltd. [Online]. Available: http://www.propsim.com

[9] B. H. Fleury, M. Tschudin, R. Heddergott, D. Dahlhaus, and K. I. Pedersen, “Channel parameter estimation in mobile radio environments using the SAGE algorithm,” *IEEE J. Select. Areas Commun.*, vol. 17, pp. 438–450, Mar.1999.

[10] Spatial Channel Model for Multiple Input Multiple Output (MIMO) Simulations (3GPP TR25.996), v6.1.0 (2003, Sept.). [Online]. Available: www.3gpp.org

[11] K. I. Pedersen, P. E. Mogensen, and B. H. Fleury, “Spatial channel characteristics in outdoor environments and their impact on BS antenna system performance,” in *Proc IEEE VTC’05*, Ottawa, Canada, vol.2, pp.719-723, 1998.

[12] L. Schumacher, K. I Pedersen, P. E. Mogensen, “From antenna spacings to theoretical capacities - guidelines for simulating MIMO systems,” in *Proc. IEEE PIMRC’2002*, vol.2, pp.587-592, Sept. 2002.

[13] W.C. Jakes, “A comparison of specific space diversity techniques for reduction of fast fading in UHF mobile radio systems,” *IEEE Trans. on Veh. Technol.*, Vol. 20, No. 4, pp. 81-92, Nov. 1971.

[14] R.W. Heath and A.J. Paulraj, “Switching between diversity and multiplexing in MIMO systems,” *IEEE Trans. Commun.*, Vol.53, Iss.6, June 2005, pp. 962- 968.

[15] D. Tse and P. Viswanath, *Fundamentals of Wireless Communication*. Cambridge University Press, 2005.

[16] L. Zheng and D. N. C. Tse, “Diversity and multiplexing: A fundamental tradeoff in multiple antenna channels,” IEEE Trans. Inf. Theory, vol.49, pp. 1073–1096, May 2003.

This full text paper was peer reviewed at the direction of IEEE Communications Society subject matter experts for publication in the IEEE "GLOBECOM" 2008 proceedings.